

Temperature-dependent photoluminescence of lead-free cesium tin halide perovskite microplates

Jiayu Tan(谭佳雨), Yixuan Zhou(周译玄), De Lu(卢德), Xukun Feng(冯旭坤), Yuqi Liu(刘玉琪),Mengen Zhang(张蒙恩), Fangzhengyi Lu(卢方正一), Yuanyuan Huang(黄媛媛), and Xinlong Xu(徐新龙)
Citation: Chin. Phys. B, 2023, 32 (**11**): 117802. DOI: 10.1088/1674-1056/ad028e
Journal homepage: http://cpb.iphy.ac.cn; http://iopscience.iop.org/cpb

What follows is a list of articles you may be interested in

Thickness-dependent excitonic properties of atomically thin 2H-$MoTe_2$

Jin-Huan Li(李金焕), Dan Bing(邴单), Zhang-Ting Wu(吴章婷), Guo-Qing Wu(吴国庆), Jing Bai(白静), Ru-Xia Du(杜如霞), Zheng-Qing Qi(祁正青)
Chin. Phys. B, 2020, 29 (**1**): 017802. DOI: 10.1088/1674-1056/ab5a3a

Temperature-dependent photoluminescence of size-tunable ZnAgInSe quaternary quantum dots

Qi Ding(丁琪), Xiao-Song Zhang(张晓松), Lan Li(李岚), Jian-Ping Xu(徐建萍), Ping Zhou(周平), Xiao-Fei Dong(董晓菲), Ming Yan(晏明)
Chin. Phys. B, 2017, 26 (**6**): 067804. DOI: 10.1088/1674-1056/26/6/067804

Temperature-dependent photoluminescence on organic-inorganicmetal halide perovskite $CH_3NH_3PbI_{3-x}Cl_x$ prepared onZnO/FTO substrates using a two-step method

Shiwei Zhuang(庄仕伟), Deqian Xu(徐德前), Jiaxin Xu(徐佳新), Bin Wu(伍斌), Yuantao Zhang(张源涛), Xin Dong(董鑫), Guoxing Li(李国兴), Baolin Zhang(张宝林), Guotong Du(杜国同)
Chin. Phys. B, 2017, 26 (**1**): 017802. DOI: 10.1088/1674-1056/26/1/017802

Influence of Al^{3+} doping on the energy levels and thermal property of the $3.5MgO{\cdot}0.5MgF_2{\cdot}GeO_2{:}Mn^{4+}$ red-emitting phosphor

Yuan Lin-lin (苑琳琳), Zhang Xiao-Song (张晓松), Xu Jian-Ping (徐建萍), Sun Jian (孙健), Jin Han (金含), Liu Xiao-Juan (刘晓娟), Li Lin-Lin (李霖霖), Li Lan (李岚)
Chin. Phys. B, 2015, 24 (**8**): 087802. DOI: 10.1088/1674-1056/24/8/087802

Fabrication and temperature-dependent photoluminescence spectra of Zn-Cu-In-S quaternary nanocrystals

Liu Xiao-Juan (刘晓娟), Zhang Xiao-Song (张晓松), Li Lan (李岚), Wang Xue-Liang (王雪亮), Yuan Lin-Lin (苑琳琳)
Chin. Phys. B, 2014, 23 (**11**): 117804. DOI: 10.1088/1674-1056/23/11/117804

SPECIAL TOPIC — Celebrating the 100th Anniversary of Physics Discipline of Northwest University

Temperature-dependent photoluminescence of lead-free cesium tin halide perovskite microplates

Jiayu Tan(谭佳雨), Yixuan Zhou(周译玄)[†], De Lu(卢德), Xukun Feng(冯旭坤), Yuqi Liu(刘玉琪), Mengen Zhang(张蒙恩), Fangzhengyi Lu(卢方正一), Yuanyuan Huang(黄媛媛), and Xinlong Xu(徐新龙)[‡]

Shaanxi Joint Laboratory of Graphene, State Key Laboratory of Photon-Technology in Western China Energy, International Collaborative Center on Photoelectric Technology and Nano Functional Materials, Institute of Photonics & Photon-Technology, School of Physics, Northwest University, Xi'an 710069, *China*

(Received 4 July 2023; revised manuscript received 13 September 2023; accepted manuscript online 12 October 2023)

Tin halide perovskites recently have attracted extensive research attention due to their similar electronic and band structures but non-toxicity compared with their lead analogues. In this work, we prepare high-quality $CsSnX_3$ (X = Br, I) microplates with lateral sizes of around 1–4 μm by chemical vapor deposition and investigate their low-temperature photoluminescence (PL) properties. A remarkable splitting of PL peaks of the $CsSnBr_3$ microplate is observed at low temperatures. Besides the possible structural phase transition at below 70 K, the multi-peak fittings using Gauss functions and the power-dependent saturation phenomenon suggest that the PL could also be influenced by the conversion from the emission of bound excitons into free excitons. With the increase of temperature, the peak position shows a blueshift tendency for $CsSnI_3$, which is governed by thermal expansion. However, the peak position of the $CsSnBr_3$ microplate exhibits a transition from redshift to blueshift at $\sim$ 160 K. The full width at half maximum of $CsSnX_3$ broadens with increasing temperature, and the fitting results imply that longitudinal optical phonons dominate the electron–phonon coupling and the coupling strength is much more robust in $CsSnBr_3$ than in $CsSnI_3$. The PL intensity of $CsSnX_3$ microplates is suppressed due to the enhanced non-radiative relaxation and exciton dissociation competing with radiative recombination. According to the Arrhenius law, the exciton binding energy of $CsSnBr_3$ is $\sim$ 38.4 meV, slightly smaller than that of $CsSnI_3$.

Keywords: cesium tin halide perovskite, temperature-dependent photoluminescence, chemical vapor deposition, microplate

PACS: 78.20.−e, 78.55.−m **DOI:** 10.1088/1674-1056/ad028e

1. Introduction

Since perovskite-type solar cells were selected as one of the ten major breakthroughs in Science in 2013, the halide perovskite materials with various components and structures have been developed significantly in the past decade in not only the photovoltaic field,[1–9] but also in optoelectronic applications, such as bright light-emitting diodes (LEDs),[10–12] low-threshold lasers,[13,14] wireless light communication,[12,15] and high-sensitivity photodetectors.[11,16,17] Being represented by lead halide perovskites, their remarkable application performances are supported by excellent optoelectronic properties, including high optical absorption coefficient,[18] long carrier lifetimes,[19] tunable narrow-band emission,[20] high fluorescence quantum efficiency,[21] and so on.[22,23] Although the performances of lead halide perovskites are outstanding, many efforts have been devoted to exploring environmentally friendly analogues with minimized performance losses.

The development of tin halide perovskites has been proved to be one of the most promising approaches because the replacement of Pb^{2+} by Sn^{2+} with a very close ionic radius can form stable perovskite structures and maintain similar electronic and band structures.[17,23–25] For example, all-inorganic cesium tin halide perovskites $CsSnX_3$ (X = Cl, Br, and I) have been reported to have excellent optoelectronic properties, such as high PL quantum efficiency,[26] tunable narrow-band PL emission,[24,27,28] high absorption coefficient,[25,29] low exciton binding energy,[24,30,31] high carrier mobility,[31] amplified spontaneous emission characteristic,[32,33] and narrower bandgaps compared with the lead analogues.[34,35] Therefore, most of the optoelectronic applications achieved by lead halide perovskites have also been demonstrated by $CsSnX_3$, including solar cells,[23,34,36] LEDs,[30] lasers,[32] and photodetectors.[28,37] However, narrowing the performance gap between tin perovskites and their lead analogues is still challenging. In order to further improve the optoelectronic performances of $CsSnX_3$, the most important foundation is the deep understanding of fundamental photophysical properties, which is still largely insufficient.

Temperature-dependent photoluminescence (PL) spectroscopy provides an effective method to investigate the photophysical properties of materials, such as exciton behaviors, thermal expansion, carrier-phonon interactions, and structural phase transition.[38–41] Many essential physical parameters

[†]Corresponding author. E-mail: yxzhou@nwu.edu.cn
[‡]Corresponding author. E-mail: xlxuphy@nwu.edu.cn

© 2023 Chinese Physical Society and IOP Publishing Ltd

can be derived by fitting the temperature dependence of the PL peak position, linewidth, and integrated intensity.[30,42–48] The temperature-dependent PL properties of various halide perovskites have been studied in recent years, and some interesting findings have been reported.[24,42,43,49–51] For instance, Wright *et al.* have proved that the scattering from longitudinal optical phonons governs the electron–phonon coupling in several hybrid lead halide perovskites.[42] The phase transitions of $MAPbBr_3$ single crystal are elucidated by Chen *et al.*[43] The splitting of the PL peaks of $CsPbBr_3$ quantum dots is investigated by Lee *et al.*[48] For $CsSnX_3$ nanocrystals, Mahesh *et al.* have reported the temperature-dependent PL features and the LED application.[30] It is worth emphasizing that the preparation method for $CsSnX_3$ is also developed in recent years. Chemical vapor deposition (CVD) has been proven to be a good way to synthesize $CsSnX_3$ micro-nano structures with excellent crystalline quality.[24,32] Particularly, the thermal PL quenching of $CsSnBr_3$ at above room temperatures has been investigated by using a micro-square and a micro-pyramid prepared by CVD.[32] Considering the important micro-laser application prospect, the temperature-dependent PL study of $CsSnX_3$ microcrystals becomes an essential but unclear subject.

In this work, high-quality $CsSnBr_3$ and $CsSnI_3$ microplates are synthesized by using the CVD method. The morphology, crystal structure, and quality of the as-prepared samples are characterized by absorption spectroscopy, x-ray diffraction (XRD), and scanning electron microscopy (SEM). The temperature-dependent steady-state PL spectra of $CsSnBr_3$ and $CsSnI_3$ microplates are measured in the range of 10 K–295 K. Obvious splitting of PL peaks of $CsSnBr_3$ is observed at the low-temperature region below 70 K, which could be induced by the structural phase transition to a lower symmetry phase. Otherwise, with multi-peak fittings using Gauss functions and the excitation power-dependent PL measurement, the sub-peaks of PL at low temperatures may also be attributed to free exciton emission and bound exciton emission with different energy. The variation of the PL peaks in peak position, linewidth, and integrated intensity are studied by curve fitting based on several theoretical models. From the linear blueshift of the PL peak position of $CsSnI_3$, the thermal expansion is clarified to take the dominating role. In comparison, the PL peak of $CsSnBr_3$ exhibits blueshift only at above 160 K, and the thermal expansion weight is much lower than that of $CsSnI_3$. From the continuous broadening of PL linewidth, as the temperature rises, the scattering of electron–phonon coupling is proved to be governed by longitudinal optical phonons. From the temperature-dependent PL intensity, the exciton binding energies of $CsSnBr_3$ and $CsSnI_3$ are derived to be 32.0 meV and 46.9 meV, respectively.

2. Experimental details

2.1. Synthesis of $CsSnX_3$ (X = Br, I) microplates

$CsSnX_3$ (X = Br, I) microplates are prepared by the CVD method on freshly cleaved mica substrates, as indicated in Fig. 1. Firstly, 26.6 mg CsBr powder (Aladdin, 99.9%) and 34.8 mg $SnBr_2$ powder (Alfa, 99.9%) (or 32.5 mg CsI powder and 46.5 mg SnI_2 powder) are mixed in an alumina boat as the precursor and placed in the center of a quartz tube furnace. The mica substrate is positioned downstream of the quartz tube in another alumina boat which is approximately 12 cm from the precursor. High-purity Ar with a flow rate of 500 sccm is held for 3 min to eliminate air in the tube. Then, the furnace is heated to the growth temperature (310 °C for $CsSnBr_3$ and 320 °C for $CsSnI_3$) for 25 min and maintained in an Ar atmosphere (20 sccm) for 30 min. At the growth temperature, CsX and SnX_2 can be carried downstream by Ar to synthesize $CsSnX_3$ on the mica substrate chemically. Lastly, the furnace is naturally cooled to room temperature with the protection of Ar flow to the sample. The temperature-dependent PL experiments are performed immediately after the samples are prepared. Then, a thin PMMA layer is spin-coated (PMMA solution, 4 wt.% in anisole, the rotational speed is 2000 rpm for 20 s) on the sample surface for further characterizations at room temperature to reduce the influence of oxidative deterioration.

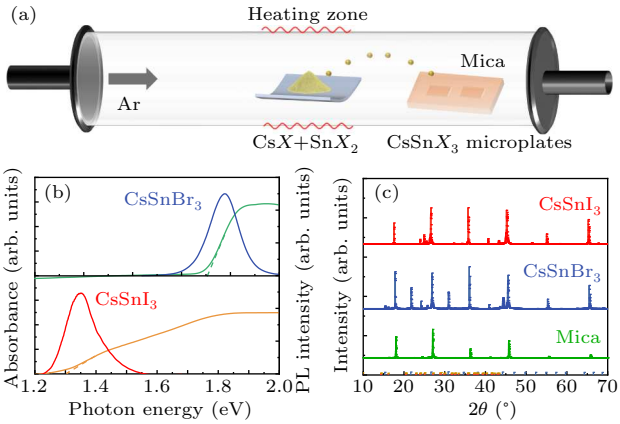


Fig. 1. (a) Schematic of the synthesis of perovskite $CsSnX_3$ microplates using the CVD method. (b) Absorption spectra and PL spectra of $CsSnX_3$ at room temperature. (c) XRD patterns.

2.2. Characterization method

The morphology and quality of the $CsSnX_3$ (X = Br, I) microplates are measured by the following experiments. The bonding configuration is confirmed by XRD (Bruker, D8 Advance). The microstructure is characterized by the SEM (Thermo Fisher, Apreo S). The optical absorption is tested by the UV-Vis absorption spectroscopy (R1, Ideaoptics).

2.3. Low-temperature PL experiments

The PL spectra are investigated by a Horiba iHR550 spectrometer with the SmartRaman confocal-micro-Raman module developed by the Institute of Semiconductors, Chinese

Academy of Sciences. In the PL measurement, the $CsSnX_3$ microplates are excited by a 532 nm laser with a power of 20 mW, which is focused by a 50× objective lens (NA = 0.55) to get a spot size of approximately 1.2 μm. With the help of a closed refrigeration system (Janis CCS-XG), PL measurements are performed in the 10 K–295 K temperature range in increments of 15 K. The $CsSnX_3$ microplates are fixed on the sample stage in a closed cycle cryogenic equipment (Janis-CCS-XG-M/204N, Janis Research Company, Inc).

3. Results and discussion

3.1. Sample characterization

The UV-Vis absorption and PL spectra of the $CsSnX_3$ microplates are investigated at room temperature, as illustrated in Fig. 1(b). According to the absorption edges, the bandgap energies of $CsSnBr_3$ and $CsSnI_3$ microplates are estimated to be 1.76 eV and 1.31 eV, respectively. Moreover, the PL spectra of these perovskite microplates show emission peaks at 1.81 eV and 1.35 eV for $CsSnBr_3$ and $CsSnI_3$ microplates, respectively. These results agree well with the previously reported bandgaps and optical bandgaps of $CsSnBr_3$ and $CsSnI_3$ samples.[24,28,30,32]

Figure 1(c) shows the XRD patterns of the $CsSnBr_3$ and $CsSnI_3$ microplates, which are compared with those of the mica substrate and type samples. The mica substrate displays a set of diffraction peaks with nearly equal spacing at $2\theta = 18.03544°$, 27.06304°, 36.2852°, 45.76029°, 55.56962°, and 65.71109°. In addition to the peaks of mica, the peaks observed at 15.40581°, 21.79045°, 26.86848°, 30.93479°, 36.07118°, 44.32054°, and 55.30156° correspond to the diffraction planes of (100), (110), (111), (200), (210), (220), and (222) for $CsSnBr_3$ with a cubic phase (JCPDS file number: 70-1645), respectively.[24,28,30] Meanwhile, the peaks at 17.86033°, 23.93894°, 24.25168°, 25.41325°, and 40.55845° correspond to the (111), (211), (121), (022), and (232) planes of orthorhombic $CsSnI_3$ (JCPDS file number: 43-1162), respectively.[24,28,30]

Figure 2 exhibits the SEM images of the as-prepared $CsSnX_3$ microplates with different magnifications. Figure 2(a) shows that $CsSnBr_3$ microplates with a high spatial density are synthesized uniformly on the flat mica substrate. Figure 2(b) gives an isolated high-quality $CsSnBr_3$ microplate with about 3.3 μm × 2.7 μm size. Note that this microplate is similar with the one used in the temperature-dependent PL experiment. From Fig. 2(c), both microplates and micro-triangles of $CsSnI_3$ can be observed on the mica substrate. These microsheets of $CsSnI_3$ have a lower density than those of $CsSnBr_3$ and a smaller average size. In the temperature-dependent PL experiment, a relatively large microplate, which is similar with the one (∼ 2.6 μm × 1.7 μm, larger than the spot size of the laser) shown in Fig. 2(d), is selected and measured. Therefore, the $CsSnBr_3$ and $CsSnI_3$ microplates used in this work have high quality and similar sizes.

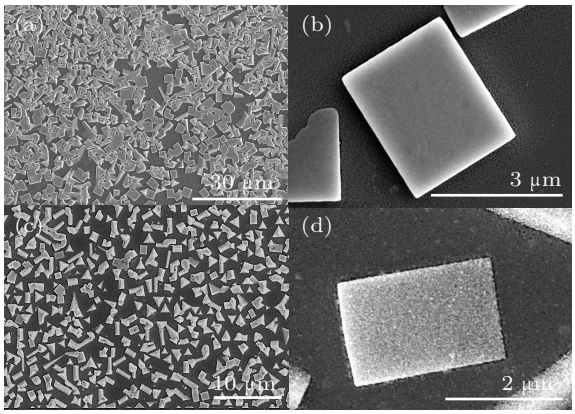


Fig. 2. SEM images of $CsSnX_3$ (X = Br, I) samples. (a) and (b) $CsSnBr_3$ microplates with different magnifications. (c) and (d) $CsSnI_3$ microplates with different magnifications.

3.2. Temperature-dependent PL

For the purpose of studying the temperature-dependent PL of $CsSnX_3$ perovskites, we record the steady-state PL spectra of $CsSnBr_3$ and $CsSnI_3$ microplates from 10 K to 295 K excited by a 532 nm continuous laser. Figures 3(a) and 3(c) show the PL spectra of $CsSnBr_3$ and $CsSnI_3$ microplates at different temperatures, respectively. For a more transparent presentation, the temperature and PL photon energy-dependent mapping of PL intensity of $CsSnBr_3$ and $CsSnI_3$ microplates are given in Figs. 3(b) and 3(d), respectively.

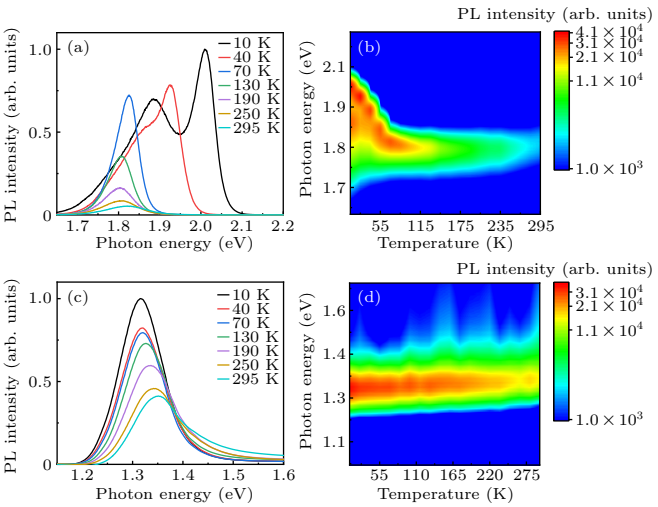


Fig. 3. Temperature-dependent PL spectra of $CsSnX_3$ microplates. (a) Steady-state PL of $CsSnBr_3$ at different temperatures. (b) Temperature and photon energy dependent mapping of the PL intensity of $CsSnBr_3$. (c) Steady-state PL of $CsSnI_3$. (d) Mapping of the PL intensity of $CsSnI_3$.

When the temperature increases from 10 K to 295 K, the PL spectra of $CsSnBr_3$ and $CsSnI_3$ microplates exhibit dramatically different properties, which can be analyzed from the following three aspects: PL peak position (optical bandgap), width at half maximum (FWHM), and integrated intensity. Generally, for both $CsSnBr_3$ and $CsSnI_3$ microplates, the PL intensity shows a decreasing tendency and the FWHM has a broadening tendency. However, compared with the consistent

blueshift tendency of the PL peak position of $CsSnI_3$, the optical bandgap of the $CsSnBr_3$ microplate exhibits a blueshift at above 160 K while a redshift at below 160 K. In addition, a remarkable splitting of the PL peaks at extremely low temperatures can be observed in Figs. 3(a) and 3(b). In the following part, we discuss the PL properties of $CsSnBr_3$ and $CsSnI_3$ microplates by splitting the PL peaks and fitting them with some theories to clarify the PL mechanism.

3.2.1. Splitting of the PL peaks of $CsSnBr_3$ at low temperatures

In the low-temperature region below 40 K, remarkable splitting of the PL peaks of the $CsSnBr_3$ microplate can be observed. In order to make the analysis easier, multi-peak fittings using Gauss functions are performed for the PL spectra below 100 K. From Fig. 4(a), at least three sub-peaks can be used to fit the experiment at 10 K well. A similar three sub-peak fitting has also been used to match the experimental results below 55 K. In the region between 70 K and 100 K, the experimental PL peak can be well-fitted by two sub-peaks. Figure 4(b) exhibits the PL curve measured at 70 K as a representative.

The possible PL mechanisms are discussed in the following part. Firstly, the dramatic change of PL peaks in this low temperature region especially between 10 K and 70 K conforms to the characteristic of structural phase transition induced PL. For example, organic halide perovskite $MAPbI_3$ has a significant shift of the PL peak at $\sim$ 160 K due to the structure changes from orthorhombic to tetragonal.[49] However, the reported structural transition temperatures of $CsSnBr_3$ are $\sim$ 270 K from orthorhombic to tetragonal and $\sim$ 300 K to cubic, which are far beyond this low-temperature region.[52–54] Recently, Gao *et al*. have reported the appearance of several new peaks and some changes in the existing modes of Raman spectrum of $CsSnBr_3$ at below 80 K, which may be induced by the instability of orthorhombic phase.[55] They claim that there may exist a phase transition to a lower symmetry (possibly monoclinic) phase at around 60 K. This phenomenon is consistent with our result, indicating that the phase transition could be a possible explanation for the peak splitting at low temperatures below 70 K. However, before the report of more direct evidence, we cannot rule out other possible mechanisms.

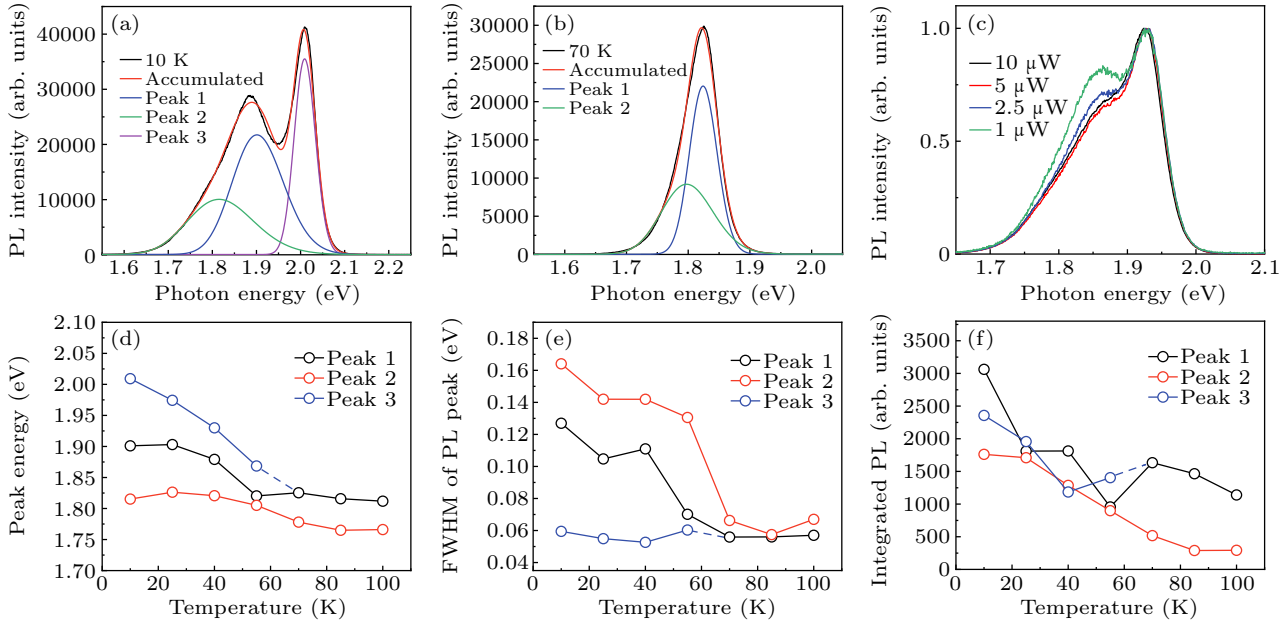


Fig. 4. Splitting of the PL peaks of $CsSnBr_3$ microplate at low temperatures. (a) PL spectrum at 10 K fitted by the sum of three Gaussian peaks. (b) PL spectrum at 70 K fitted by the sum of two Gaussian peaks. (c) PL spectra at 40 K with different excitation power. (d) Temperature-dependent peak energies extracted from the PL spectra. (e) Temperature-dependent FWHM. (f) Temperature-dependent integrated PL intensity.

Secondly, we try to understand the PL mechanism beyond the phase transition by analyzing the temperature-dependent sub-peak properties obtained in Fig. 4. Take the 10 K condition as an example (Fig. 4(a)), the positions of sub-peaks are at 2.01 eV (peak 3), 1.90 eV (peak 1), and 1.82 eV (peak 2), corresponding to different FWHM values of 17.5 meV, 46.7 meV, and 66.2 meV, respectively. Note that peaks 1 and 2 merge into a wide peak which cannot be fitted with a single Gauss function well, while peak 3 is separated and sharp. Because the characteristic thermal energy is much lower than the exciton binding energy, these sub-peaks could be induced by the radiative recombination of free excitons and bound excitons. Compared with free exciton emission, the peaks of bound exciton emission are usually broadened by the numerous binding sites to defects.[56] Therefore, it can be speculated that peaks 1 and 2 may be largely contributed by the bound exciton emission. This assumption is confirmed by the excitation power-dependent PL measurements. Figure 4(c) shows the power dependence of the PL spectra at 40 K as a representative. The PL intensity is normalized by the maximum value of peak 3.

When the excitation power increases from 1 μW to 10 μW, the PL intensity ratio of the wide peak decreases and becomes saturated, which is a typical characteristic of bound exciton emission.[43,49] Therefore, peaks 1 and 2 at below 40 K are proved to be related to the bound exciton emission, and peak 3 is not induced by bound excitons.

Figures 4(d)–4(f) show the temperature-dependent peak position, FWHM, and integrated intensity extracted from the PL sub-peaks, respectively. From Fig. 4(d), redshift is observed for all three sub-peaks, and the trend is more significant at below 70 K. Then, the separated peak 3 merges into peaks 1 and 2 at ∼ 70 K. However, the total peak is still asymmetric, so at least two sub-peaks are needed to fit the experiment at above 70 K. Here, the redshift of peak energies could be induced by the exciton–phonon interaction,[46] which is a common reason for the PL peak position shift to lower energy. However, since the redshift trend is more significant at below 70 K, where the phonon effects may be suppressed, we believe the peak shift could also be induced by the transition of bound exciton emission with a wide energy range to free exciton emission. As supported by Fig. 4(e), the FWHM of peaks 1 and 2, which are attributed to bound excitons with different energies, narrows dramatically at below 70 K and become stable at higher temperatures. From Fig. 4(f), the sum of integrated PL intensity of peaks 1 and 2 is much larger than that of peak 3 at 10 K, indicating that the PL is governed by bound exciton emission at very low temperatures. These results suggest that the dominant PL mechanism of $CsSnBr_3$ changes from bound exciton emission to free exciton emission as temperature increases from 10 K to 70 K.

3.2.2. Splitting of the PL peaks of $CsSnBr_3$ and $CsSnI_3$

In the range from 70 K to 295 K, temperature-dependent PL properties of the $CsSnBr_3$ microplate are analyzed, as shown in Fig. 5. Splitting the PL peaks is performed by fitting with two Gaussian peaks. Compared with the low-temperature condition of 70 K (Fig. 4(b)), the side peak (peak 2) exhibits a greatly reduced influence on the main peak (peak 1) at 250 K, as shown in Fig. 5(a). The evolution of the PL peak positions as temperature rises is given in Fig. 5(b). Peak 2 exhibits a redshift trend in the whole range. However, a remarkable transition from redshift to blueshift of peak 1 is observed, indicating a complex PL mechanism. Figure 5(c) shows the temperature-dependent FWHM of peaks 1 and 2. The former appears to have an obviously broadening tendency, while the latter is relatively stable. The integrated PL intensity of peak 1 relative to that of peak 2 is shown in Fig. 5(d). The largely enhanced intensity ratio implies that the contribution from peak 2 is gradually weakened with the increase of temperature. Here, the main and the side peaks are attributed to the band-edge and defect states, respectively. The dominant PL mechanisms for the change of the main peak are discussed in the last part with curve fitting.

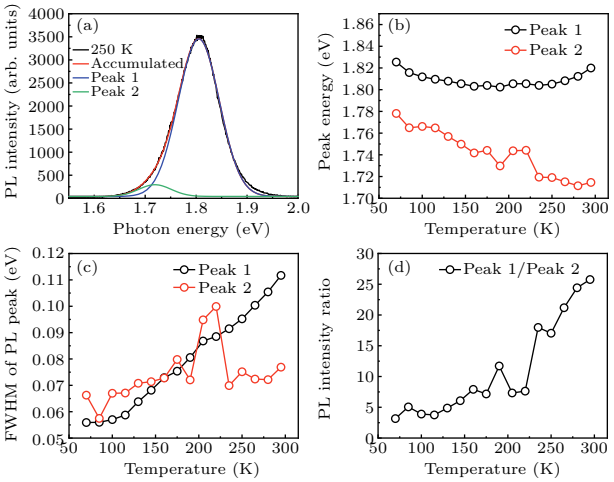


Fig. 5. Temperature-dependent PL properties of $CsSnBr_3$ in the range of 70 K–295 K. (a) Splitting of the PL peaks of $CsSnBr_3$ microplate at 250 K fitted by the sum of two Gaussian peaks. (b) PL peak energies of peak 1 and peak 2. (c) FWHM of peak 1 and peak 2. (d) Integrated PL intensity ratio of peak 1 relative to that of peak 2.

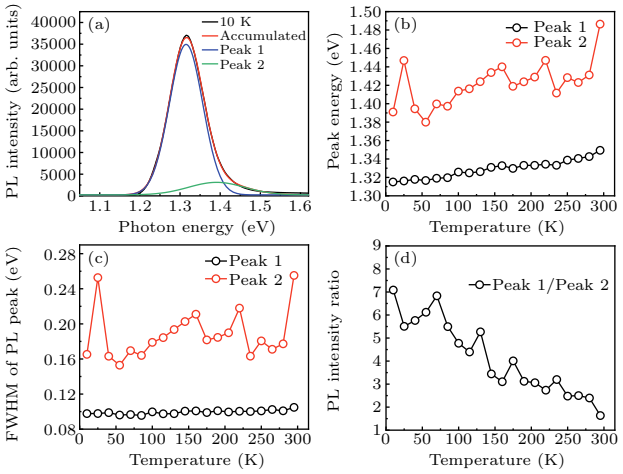


Fig. 6. Temperature-dependent PL properties of $CsSnI_3$ at the range of 10 K–295 K. (a) Splitting of the PL peaks of $CsSnI_3$ microplate at 10 K fitted by the sum of two Gaussian peaks. (b) PL peak energies of peak 1 and peak 2. (c) FWHM of peak 1 and peak 2. (d) Integrated PL intensity ratio of peak 1 relative to that of peak 2.

In comparison, the temperature-dependent PL peaks of the $CsSnI_3$ microplate in the range from 10 K to 295 K are given in Fig. 6. Because the PL spectra of $CsSnI_3$ also exhibit asymmetry, especially at near room temperatures, the experiments are fitted by the sum of two Gaussian peaks. For example, the splitting of the PL peak at 10 K is given in Fig. 6(a). Moreover, the temperature-dependent PL peak position, FWHM of peaks, and integrated PL intensity ratio of peak 1/peak 2 are shown in Figs. 6(b)–6(d), respectively. Here, the $CsSnI_3$ microplate shows quite different temperature-dependence of the PL properties. (i) In the low-temperature region between 10 K to 100 K, the side peak is extremely weak and no obvious broadening of peak 1 is observed, indicating no significant bound exciton emission like in $CsSnBr_3$. (ii) The peak energy of peak 2 is larger than

that of the main peak, which is opposite to the condition of $CsSnBr_3$. Moreover, only blueshift of peak 1 is obtained for $CsSnI_3$ as the rise of temperature, suggesting a different dominant mechanism. (iii) The broaden tendency of the FWHM of peak 1 is much weaker than that of $CsSnBr_3$, implying a reduced electron–phonon coupling. (iv) The PL intensity ratio of peak 1/peak 2 reduces gradually, resulting in an enhanced asymmetry at near-room temperatures. Similar phenomena have also been covered in other reports.[45,57,58] Therefore, the PL mechanism of the side peak of $CsSnI_3$ should be different from that of $CsSnBr_3$. According to Yu's report, this asymmetric broadening may be caused by factors such as composition fluctuations and granular boundaries.[45] The changing mechanism of the main PL peak is discussed in the following part.

3.2.3. Fitting of temperature-dependent PL peaks

As shown in Fig. 7, the temperature dependence of the PL peak energy, FWHM, and integrated intensity of the main peaks of $CsSnBr_3$ and $CsSnI_3$ microplates are studied by curve fitting based on some widely acknowledged theory models. As a result, many critical physical parameters are calculated, as given in Table 1. The detailed fitting processes and mechanism discussions are as follows.

Table 1. Curve fitting parameters of $CsSnX_3$ microplates.

Sample	E_b (meV)	E_0 (eV)	Γ_0 (meV)	γ_{LO} (meV)	E_{LO} (meV)
$CsSnBr_3$	32.0	1.79	56.2	166.0	35.1
$CsSnI_3$	46.9	1.31	96.3	18.0	31.2

Firstly, the temperature-dependent shift of the PL peak position is discussed. Figure 7(a) shows that redshift and blueshift tendencies of the $CsSnBr_3$ microplate can be observed in temperature regions below and above 160 K, respectively. For the $CsSnI_3$ microplate, a consistent blueshift tendency of the PL peak position can be observed in Fig. 7(b). For conventional semiconductors, the PL peak energy E_g is usually described by an empirical relation as $E_g(T) = E_0 - \alpha T^2/(T+\beta)$,[40] where E_0 is the unrenormalized bandgap, α and β are fitting parameters. This relation reveals a decrease in bandgap as temperature increases, which is usually influenced by electron–phonon interactions. However, this tendency is inconsistent with the blueshift of our perovskite samples. Meanwhile, the blueshift phenomena have been reported by many other lead-based perovskites,[42,45,48,51] in which the temperature-dependent bandgap is attributed to the following two factors: change of the lattice constant induced by thermal expansion; renormalization of the bandgap energies driven by electron–phonon interactions.[38,59–61] The former arises from the anharmonicity of the inter-atomic potentials. The latter consists of Fan[39] and Debye–Waller[62,63] terms, describing the virtual phonon emission/absorption processes and the interactions of an electron with two phonons with opposite wave vectors at the branch j, respectively. Therefore, the temperature dependence of the bandgap can be estimated by two terms[45]

$$\frac{\partial E_g}{\partial T} = \frac{\partial E_g}{\partial V}\frac{\partial V}{\partial T} + \sum_{j,\boldsymbol{q}}\left(\frac{\partial E_g}{\partial n_{j,\boldsymbol{q}}}\right)\left(n_{j,\boldsymbol{q}} + \frac{1}{2}\right), \tag{1}$$

where $n_{j,\boldsymbol{q}}$ is the phonon mode number at the branch j with wave vector $\boldsymbol{q}$ and follows the Bose–Einstein distribution. This equation can be further simplified based on the one-oscillator model as[45,46,51]

$$E_g(T) = E_0 + A_{TE}T + A_{EP}\left(\frac{2}{\exp\left(\frac{\hbar\omega}{kT}\right) - 1} + 1\right), \tag{2}$$

where $\hbar\omega$ is the average optical phonon energy, A_{TE} and A_{EP} are the weight of thermal expansion and electron–phonon interaction, respectively. As shown in Fig. 7(b), the fitting line agrees well with the experiment of $CsSnI_3$, and a linear dependence with a coefficient of 0.11 meV/K is obtained. The E_0 parameter of the $CsSnI_3$ microplate is calculated to be ~ 1.31 eV, which is close to the previous report.[45] The absence of A_{EP} implies that the contribution of electron–phonon interaction to the bandgap change is negligible, which could be attributed to the large effective mass of electrons in $CsSnI_3$. Therefore, the temperature-dependent bandgap of $CsSnI_3$ is dominated by the thermal expansion effect. However, the PL peak position changes of the $CsSnBr_3$ microplate cannot be fitted well by this equation in the whole experimental temperature range due to the extraordinary redshift below 160 K and the increasing slope of blueshift at above ~ 265 K. Therefore, the study on the temperature-dependent bandgap is carried out in different temperature regions. As shown in Fig. 7(a), the fitting line calculated based on Eq. (2) shows a good agreement with the experiment in the temperature range between 160 K and 265 K. Here, the electron–phonon interaction term also plays a negative role so the linear blueshift is governed by the thermal expansion. The E_0 parameter is calculated to be ~ 1.79 eV and A_{TE} coefficient is ~ 0.05 meV/K, which is much lower than that of $CsSnI_3$. In the low temperature region below 160 K, we believe the slight redshift (compared with the obvious blueshift of $CsSnI_3$) is influenced by the renormalization of bandgap, which might be induced by the above-mentioned structural phase transition or the transition from bound exciton emission into free exciton emission at below 70 K. These processes could be dominant at below 70 K and not be ignored at below 160 K. At above 265 K, it has been reported that a phase transition from orthorhombic to tetragonal could occur in $CsSnBr_3$ at around 270 K.[52] Therefore, the increasing slope of the PL peak at 265 K–295 K may be attributed to the enhanced weight of thermal expansion due to the different structural phase.[46]

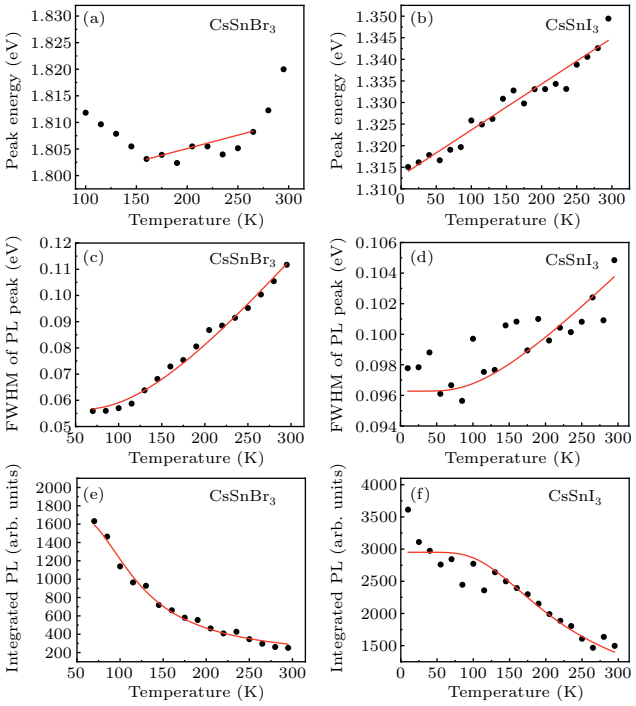


Fig. 7. Temperature-dependent PL properties of CsSnX_3 microplates. (a) and (b) PL peak energy. (c) and (d) FWHM. (e) and (f) Integrated PL intensity.

Secondly, the temperature dependence of the FWHM and the underlying mechanism is discussed. From Figs. 7(c) and 7(d), the FWHM of $CsSnBr_3$ and $CsSnI_3$ microplates broadens with increasing temperature. Generally, this PL broadening is related to the electron–phonon coupling in inorganic semiconductors, such as the different scattering processes between charge carriers and phonons (or impurities), which have different dependencies on temperature.[38,41,64,65] According to the report by Wright *et al.*,[42] the temperature-dependent PL linewidth Γ can be given as

$$\Gamma(T) = \Gamma_0 + \gamma_{ac} T + \frac{\gamma_{LO}}{e^{\frac{E_{LO}}{kT}} - 1} + \gamma_{imp} e^{-\frac{E_{imp}}{kT}}, \tag{3}$$

where Γ_0 is a temperature-independent inhomogeneous broadening term induced by scattering of disorder and imperfections; γ_{ac} is defined as the coupling strength between charge carriers and acoustic phonons; γ_{LO} is the coupling strength between charge carriers and longitudinal optical phonons; E_{LO} is the energy of longitudinal optical phonons; γ_{imp} is attributed to the scattering of impurities; E_{imp} is the average binding energy of impurities. In the fitting of both $CsSnBr_3$ and $CsSnI_3$, the γ_{ac} and γ_{imp} terms are set as zero according to the citation,[42] and the calculated lines agree well with the experiments, as shown in Figs. 7(c) and 7(d). This result suggests that the electron–phonon coupling in CsSnX_3 microplates is dominated by the interaction between charge carriers and longitudinal optical phonons, which is consistent with the conclusion obtained in MAPbX_3 and FAPbX_3 perovskites.[42] Moreover, the fitting parameters of the $CsSnBr_3$ microplate are $\Gamma_0 = 56.2$ meV, $\gamma_{LO} = 166.0$ meV, and $E_{LO} = 35.1$ meV, and of the $CsSnI_3$ microplate are $\Gamma_0 = 96.3$ meV, $\gamma_{LO} = 18.0$ meV, and $E_{LO} = 31.2$ meV. Compared with $CsSnI_3$, the coupling strength in the $CsSnBr_3$ microplate appears much more robust, which could be induced by the smaller high-frequency value of the dielectric function in $CsSnBr_3$ than in $CsSnI_3$.[42]

Lastly, the temperature dependence of the integrated PL intensity of $CsSnBr_3$ and $CsSnI_3$ microplates are discussed according to the experimental data plotted in Figs. 7(e) and 7(f), respectively. Here, a continuous decreasing trend is observed for both $CsSnBr_3$ and $CsSnI_3$ as the temperature rises. According to the literature, the relationship between the integrated PL intensity I and temperature T can be described by the Arrhenius equation as[44,47,48,51,66–69]

$$I(T) = \frac{I_0}{1 + A e^{-\frac{E_b}{kT}}}, \tag{4}$$

where I_0 is the integrated PL intensity at 0 K, A is the pre-exponential coefficient, E_b is the exciton binding energy, and k is the Boltzmann constant. From Figs. 7(a) and 7(b), the red fitting lines agree well with the experiments, indicating that the E_b values are estimated to be 32.0 meV and 46.9 meV for $CsSnBr_3$ and $CsSnI_3$ microplates, respectively. The continuous decrease of the PL intensity suggests that the radiative recombination is gradually suppressed by the thermal activation of exciton dissociation or non-radiative relaxation. The exciton binding energy of the $CsSnBr_3$ microplate is lower than that of the $CsSnI_3$ microplate.

4. Conclusion

High-quality CsSnX_3 (X = Br, I) microplates are prepared by CVD and characterized by XRD, SEM, and absorption spectroscopy. The temperature-dependent steady-state PL spectra of the samples are investigated in the range of 10 K–295 K. At the low-temperature region, the remarkable splitting of PL peaks of the $CsSnBr_3$ microplate is speculated to be induced by structural phase transition or the coexistence of free exciton emission and bound exciton emission with different energies. The temperature-dependent characteristics of PL intensity decline, peak position shift, and linewidth broadening are analyzed by curve fitting using several theoretical models. Moreover, several important physical parameters, such as exciton binding energy, unrenormalized bandgap, and coupling strength of longitudinal optical phonons, have been estimated from the fitting. Compared with the obvious linear blueshift of the PL peak energy of $CsSnI_3$, the slight blueshift takes the leading role at above $\sim$ 160 K in the PL of $CsSnBr_3$, indicating that the thermal expansion weight is much stronger in $CsSnI_3$ than in $CsSnBr_3$. The scattering of longitudinal optical phonons is proved to dominate the electron–phonon coupling in $CsSnBr_3$ and $CsSnI_3$, but the coupling strength in $CsSnBr_3$

is more significant than that in $CsSnI_3$. This research provides an insight into the photophysical properties of $CsSnX_3$ microplates, which is essential for tin perovskite-based optoelectronic applications, especially for developing micro-lasers.

Acknowledgment

Project supported by the National Natural Science Foundation of China (Grant Nos. 11974279, 12074311, 12004310, and 12261141662).

References

[1] Etgar L, Gao P, Xue Z, Peng Q, Chandiran A K, Liu B, Nazeeruddin M K and Gratzel M 2012 *J. Am. Chem. Soc.* **134** 17396
[2] Ball J M, Lee M M, Hey A and Snaith H J 2013 *Energy Environ. Sci.* **6** 1739
[3] Bi D, Yang L, Boschloo G, Hagfeldt A and Johansson E M 2013 *J. Phys. Chem. Lett.* **4** 1532
[4] Heo J H, Im S H, Noh J H, Mandal T N, Lim C S, Chang J A, Lee Y H, Kim H J, Sarkar A, Nazeeruddin M K, Grätzel M and Seok S I 2013 *Nat. Photonics* **7** 486
[5] Kim H S, Lee J W, Yantara N, Boix P P, Kulkarni S A, Mhaisalkar S, Gratzel M and Park N G 2013 *Nano Lett.* **13** 2412
[6] Laban W A and Etgar L 2013 *Energy Environ. Sci.* **6** 3249
[7] Jishi R A, Ta O B and Sharif A A 2014 *J. Phys. Chem. C* **118** 28344
[8] Yang W S, Park B W, Jung E H, Jeon N J, Kim Y C, Lee D U, Shin S S, Seo J, Kim E K, Noh J H and Seok S I 2017 *Science* **356** 1376
[9] Liu X, Wu T, Luo X, Wang H, Furue M, Bessho T, Zhang Y, Nakazaki J, Segawa H and Han L 2021 *ACS Energy Lett.* **7** 425
[10] Cao Y, Wang N, Tian H, *et al.* 2018 *Nature* **562** 249
[11] Dou L, Yang Y M, You J, Hong Z, Chang W H, Li G and Yang Y 2014 *Nat. Commun.* **5** 5404
[12] Mo Q, Yu J, Chen C, Cai W, Zhao S, Li H and Zang Z 2022 *Laser Photonics Rev.* **16**
[13] Fu Y, Zhu H, Chen J, Hautzinger M P, Zhu X Y and Jin S 2019 *Nat. Rev. Mater.* **4** 169
[14] Fu Y, Zhu H, Stoumpos C C, Ding Q, Wang J, Kanatzidis M G, Zhu X and Jin S 2016 *ACS Nano* **10** 7963
[15] Zhao S, Jia Z, Huang Y, Qian Q, Lin Q and Zang Z 2023 *Adv. Funct. Mater.* 2305858
[16] Yakunin S, Dirin D N, Shynkarenko Y, Morad V, Cherniukh I, Nazarenko O, Kreil D, Nauser T and Kovalenko M V 2016 *Nat. Photonics* **10** 585
[17] Gao Y, Pan Y, Zhou F, Niu G and Yan C 2021 *J. Mater. Chem. A* **9** 11931
[18] De Wolf S, Holovsky J, Moon S J, Loper P, Niesen B, Ledinsky M, Haug F J, Yum J H and Ballif C 2014 *J. Phys. Chem. Lett.* **5** 1035
[19] Shi D, Adinolfi V, Comin R, Yuan M, Alarousu E, Buin A, Chen Y, Hoogland S, Rothenberger A, Katsiev K, Losovyj Y, Zhang X, Dowben P A, Mohammed O F, Sargent E H and Bakr O M 2015 *Science* **347** 519
[20] Zhu H, Fu Y, Meng F, Wu X, Gong Z, Ding Q, Gustafsson M V, Trinh M T, Jin S and Zhu X Y 2015 *Nat. Mater.* **14** 636
[21] Protesescu L, Yakunin S, Bodnarchuk M I, Krieg F, Caputo R, Hendon C H, Yang R X, Walsh A and Kovalenko M V 2015 *Nano Lett.* **15** 3692
[22] Faheem M B, Khan B, Feng C, Farooq M U, Raziq F, Xiao Y and Li Y 2019 *ACS Energy Lett.* **5** 290
[23] Duan C, Zhao Z and Yuan L 2021 *IEEE J. Photovolt.* **11** 1126
[24] Chen J, Luo Z, Fu Y, Wang X, Czech K J, Shen S, Guo L, Wright J C, Pan A and Jin S 2019 *ACS Energy Lett.* **4** 1045
[25] Kang C, Rao H, Fang Y, Zeng J, Pan Z and Zhong X 2021 *Angew. Chem. Int. Ed.* **60** 660
[26] Wang L M, Chen J K, Zhang B B, Liu Q, Zhou Y, Shu J, Wang Z, Shirahata N, Song B, Mohammed O F, Bakr O M and Sun H T 2021 *Nanoscale* **13** 16726
[27] Jellicoe T C, Richter J M, Glass H F, Tabachnyk M, Brady R, Dutton S E, Rao A, Friend R H, Credgington D, Greenham N C and Bohm M L 2016 *J. Am. Chem. Soc.* **138** 2941
[28] Han M, Sun J, Peng M, Han N, Chen Z, Liu D, Guo Y, Zhao S, Shan C, Xu T, Hao X, Hu W and Yang Z X 2019 *J. Phys. Chem. C* **123** 17566
[29] Peedikakkandy L and Bhargava P 2016 *RSC Adv.* **6** 19857
[30] Mahesh K P O, Chang C Y, Hong W L, Wen T H, Lo P H, Chiu H Z, Hsu C L, Horng S F and Chao Y C 2020 *RSC Adv.* **10** 37161
[31] Huang L Y and Lambrecht W R L 2013 *Phys. Rev. B* **88** 165203
[32] Wu Z Y, Zhuang J H, Lin Y T, Chou Y H, Wu P C, Wu C L, Chen P and Hsu H C 2021 *ACS Nano* **15** 19613
[33] Xing G, Kumar M H, Chong W K, Liu X, Cai Y, Ding H, Asta M, Gratzel M, Mhaisalkar S, Mathews N and Sum T C 2016 *Adv. Mater.* **28** 8191
[34] Gupta S, Bendikov T, Hodes G and Cahen D 2016 *ACS Energy Lett.* **1** 1028
[35] Song T B, Yokoyama T, Aramaki S and Kanatzidis M G 2017 *ACS Energy Lett.* **2** 897
[36] Moghe D, Wang L, Traverse C J, Redoute A, Sponseller M, Brown P R, Bulović V and Lunt R R 2016 *Nano Energy* **28** 469
[37] Xu W L, Yuan H, Yang X Y, Zhang Y and Zheng M 2021 *Physica E* **134** 114843
[38] O'donnell K P and Chen X 1991 *Appl. Phys. Lett.* **58** 2924
[39] Fan H Y 1951 *Phys. Rev.* **82** 900
[40] Varshni Y P 1967 *Physica* **34** 149
[41] Rudin S and Reinecke T L 1990 *Phys. Rev. B* **41** 3017
[42] Wright A D, Verdi C, Milot R L, Eperon G E, Perez-Osorio M A, Snaith H J, Giustino F, Johnston M B and Herz L M 2016 *Nat. Commun.* **7** 11755
[43] Chen C, Hu X, Lu W, Chang S, Shi L, Li L, Zhong H and Han J B 2018 *J. Phys. D: Appl. Phys.* **51** 045105
[44] Jiang D S, Jung H and Ploog K 1988 *J. Appl. Phys.* **64** 1371
[45] Yu C, Chen Z J, Wang J, Pfenninger W, Vockic N, Kenney J T and Shum K 2011 *J. Appl. Phys.* **110** 063526
[46] Wei K, Xu Z, Chen R, Zheng X, Cheng X and Jiang T 2016 *Opt. Lett.* **41** 3821
[47] Wu K, Bera A, Ma C, Du Y, Yang Y, Li L and Wu T 2014 *Phys. Chem. Chem. Phys.* **16** 22476
[48] Lee S M, Moon C J, Lim H, Lee Y, Choi M Y and Bang J 2017 *J. Phys. Chem. C* **121** 26054
[49] Fang H H, Raissa R, Abdu-Aguye M, Adjokatse S, Blake G R, Even J and Loi M A 2015 *Adv. Funct. Mater.* **25** 2378
[50] Wehrenfennig C, Liu M, Snaith H J, Johnston M B and Herz L M 2014 *APL Mater.* **2** 081513
[51] Diab H, Trippe-Allard G, Ledee F, Jemli K, Vilar C, Bouchez G, Jacques V L, Tejeda A, Even J, Lauret J S, Deleporte E and Garrot D 2016 *J. Phys. Chem. Lett.* **7** 5093
[52] Fabini D H, Laurita G, Bechtel J S, Stoumpos C C, Evans H A, Kontos A G, Raptis Y S, Falaras P, Van Der Ven A, Kanatzidis M G and Seshadri R 2016 *J. Am. Chem. Soc.* **138** 11820
[53] Singh S, Kumar M, Jha P K, Jha P A and Singh P 2023 *Europhys. Lett.* **141** 26001
[54] Mori M and Saito H 1986 *J. Phys. C: Solid State Phys.* **19** 2391
[55] Gao L, Yadgarov L, Sharma R, Korobko R, Mccall K M, Fabini D H, Stoumpos C C, Kanatzidis M G, Rappe A M and Yaffe O 2021 *Mater. Adv.* **2** 4610
[56] Korn T, Heydrich S, Hirmer M, Schmutzler J and Schüller C 2011 *Appl. Phys. Lett.* **99** 102109
[57] Shum K, Chen Z, Qureshi J, Yu C, Wang J J, Pfenninger W, Vockic N, Midgley J and Kenney J T 2010 *Appl. Phys. Lett.* **96** 221903
[58] Kontos A G, Kaltzoglou A, Arfanis M K, Mccall K M, Stoumpos C C, Wessels B W, Falaras P and Kanatzidis M G 2018 *J. Phys. Chem. C* **122** 26353
[59] Allen P B and Cardona M 1983 *Phys. Rev. B* **27** 4760
[60] Lautenschlager P, Allen P B and Cardona M 1985 *Phys. Rev. B: Condens. Matter* **31** 2163
[61] Göbel A, Ruf T, Cardona M, Lin C T, Wrzesinski J, Steube M, Reimann K, Merle J C and Joucla M 1998 *Phys. Rev. B* **57** 15183
[62] Vicena F 1955 *Czechoslov. J. Phys.* **5** 499
[63] Keffer C, Hayes T M and Bienenstock A 1968 *Phys. Rev. Lett.* **21** 1676
[64] Cardona M 2005 *Solid State Commun.* **133** 3
[65] Lee J, Koteles E S and Vassell M O 1986 *Phys. Rev. B* **33** 5512
[66] Sun S, Salim T, Mathews N, Duchamp M, Boothroyd C, Xing G, Sum T C and Lam Y M 2014 *Energ. Environ. Sci.* **7** 399
[67] Yangui A, Pillet S, Mlayah A, Lusson A, Bouchez G, Triki S, Abid Y and Boukheddaden K 2015 *J. Chem. Phys.* **143** 224201
[68] Fujisawa J I and Ishihara T 2004 *Phys. Rev. B* **70** 205330
[69] Ishihara T, Takahashi J and Goto T 1990 *Phys. Rev. B* **42** 11099